Wilde-Piórko M, Duda SJ, Grad M. 地震和爆炸的 P 波层析成像──第二部分：由时频地震图得到的 2004 年苏门答腊-安达曼地震的断层破裂特征[J]. CT 理论与应用研究, 2011, 20(4): 465-483.
Wilde-Piórko M, Duda SJ, Grad M. Tomography of seismic P-waves from earthquakes and explosions — Part II: Morphology of faulting of the 2004 Sumatra-Andaman earthquake from spectral seismograms[J]. CT Theory and Applications, 2011, 20(4): 465-483.

Tomography of Seismic P-Waves from Earthquakes and Explosions
— Part II: Morphology of Faulting of the 2004 Sumatra-Andaman Earthquake from Spectral Seismograms

Monika WILDE-PIÓRKO[1], Seweryn J. DUDA[2✉], Marek GRAD[1]

1. Institute of Geophysics, Faculty of Physics, University of Warsaw, Pasteura 7, 02-093 Warsaw, Poland
2. Institute of Geophysics, Hamburg University, Bundesstrasse 55, 20146 Hamburg, Germany

Abstract: The paper is concerned with the analysis of broadband seismograms of the Sumatra-Andaman earthquake of 26 December 2004. The purpose of the analysis is to recognize the morphology of the faulting process in terms of the time of occurrence and of the frequency content of subevents. The analysis is based on spectral seismograms of P-waves, obtained from the corresponding broadband recordings. It is found that 15 major subevents with maximum radiation intensity at frequencies lower than about 1 Hz occurred during the time window prior to the arrival of the major S-wave. In the same time window however hundreds of subevents took place with maximum radiation intensity at higher frequencies, producing a quasi-continuous “humming” at infrasonic frequencies observable at distances of the order of 8 000 km. In view of the strong absorption of the high frequency waves during the propagation along the ray path, it may be concluded that the “humming” reflects a substantial portion of the seismic energy released during the earthquake.

Key words: Sumatra-Andaman earthquake; broadband seismograms; spectral seismograms; high-frequent radiation of seismic energy; duration of faulting

Article ID: 1004-4140（2011）04-0465-19 **CLC Number:** P 315 **Document code:** A

The present paper outlines results of a study whose earlier outcome was given in the paper by Duda[1]. The earlier publication contains basics of the application of spectral seismograms to broadband records of earthquakes and explosions. In the present paper the method is applied to the analysis of broadband seismograms of the Sumatra-Andaman earthquake.

The aim of the present study is to decipher the morphology of faulting understood as the temporal succession of events contributing to the earthquake, together with the spectral composition of the waves radiated from individual subevents. Each one of the subevents, especially the largest one, may be considered as earthquakes of their own, the subevent occurring within a “short” time interval and being located in “close” proximity. The individual

Received Date: 2011-05-31.

quantification of the subevents poses formidable difficulties, and no ready method is available for the solution of the problem. Consequently in seismological practice — as far as the earthquake parameters are concerned — one limits oneself usually to the determination of one set of coordinates of the focus, one magnitude and/or seismic moment of the earthquake etc, while each one of the subevents would deserve a respective individual treatment. The present study is devoted to the recognition of individual characteristics of subevents, found from broadband recordings at teleseismic distances.

The present analysis of the Sumatra-Andaman earthquake of 26 December 2004 — one of the most significant and best-recorded earthquakes — emphasizes the early part of broadband seismograms, in which detailed information on the rupturing history is expected. A procedure is presented for recognizing the temporal history of the faulting process of earthquakes. The Sumatra-Andaman earthquake is discussed on the background of five reference earthquakes selected from the strongest earthquakes that have occurred in the region in the time since the event of 26 December 2004.

The Sumatra-Andaman earthquake is not only one of the strongest events ever recorded on seismographs (Its strength is apparently exceeded only by that of the Chilean 1960 and the Alaska 1964 earthquakes.), but it was also recorded on a larger number of seismographs than any earlier earthquake. The seismographs — especially digitally recording broadband, wide dynamic range seismographs — feature highest recording quality of seismic waves achieved to date. In principle, broadband, wide dynamic range seismographs offer better possibilities than conventional instruments to recognize features of the faulting process and to quantify these features by way of suitable parameters. A limit is set however by the transparency of the medium — relative to the radiation intensity of the given seismic wave at a given frequency — between the fault and the seismograph site. The transparency is thereby controlled primarily by the velocity heterogeneity and the anelasticity of the Earth material. Another limit to recognize features of the faulting process results from the radiation and the propagation of seismic waves themselves: due to a multitude of successive rupturing episodes occurring in general during earthquakes and due to multipathing of waves radiated during each one of these episodes, the phases overlap, and disentangling is a serious problem.

The aim of the present study is to recognize and quantify individual bursts of seismic energy contributing to the Sumatra-Andaman earthquake in a broad band of frequencies and over a wide dynamic range below that of the strongest burst. The energy bursts, as far as they are recognizable, are quantified with respect to their arrival times, their relative strengths and their frequency contents.

1 The Sumatra-Andaman earthquake

Table 1 summarizes the parameters of the Sumatra-Andaman earthquake published by the US Geological Survey-National Earthquake Information Center (World Data Center-). The respective values are considered to be the most reliable ones, within the error limits, if given. Added are a few values from additional sources, as indicated. The focal depth was assumed by USGS-NEIC to be 30 km (10 km by the Incorporated Research Institutions for Seismology, IRIS), i.e. with nearly 500 stations available it was not possible to identify seismic phases suitable for depth determination. The epicentral coordinates and the focal depth, as also the origin time, refer to the point of initial rupture in the Earth's crust. Subsequent studies have shown that the entire rupture extended for more than 1 000 km in the north-westerly direction

and apparently continued for about 10 min. See Ammon et al[2], Banerjee et al[3], Park et al[4], Lay et al[5], Gusev et al[6], Liu et al[7].

Table 1 Parameters of the Sumatra-Andaman earthquake

Column Name	Column Name
Date	26 December 2004
Origin time	00:58:53.50 UTC
Epicentral coordinates	3.30°N, 95.98°E
Error estimate in horizontal	+5.9 km
Focal depth (fixed by location program)	30 km (IRIS 10 km)
Number of stations available for the determination of the epicentral coordinates and focal depth	488
Distance from epicenter to nearest seismic station available	643.4 km; 5.8°
Root-mean-square error of arrival times of first P-wave	1.16 s
Largest gap in azimuthal coverage by seismic stations available	28.7°
Magnitude M_w (teleseismic moment magnitude)	9.1 (IRIS 8.5)
Duration of faulting	8~10.5 min (Gusev et al[6])
Epicentral distance to station LBTB	73.7°; 8 181 km

The parameter values were published by USGS-NEIC (WDCS-D), unless mentioned otherwise

Table 2 Basic parameters of five reference earthquakes to the Sumatra-Andaman earthquake of 2010-12-26, 00:58:53.50 UTC

Date	Origin time	Epicentral coordinates	Focal depth /km	Magnitude M_w	Epicentral distance to station LBTB/°
2004-12-26	21:29.8	6.91°N, 92.96°E	39	7.2	72.8
2005-03-28	09:36.5	2.09°N, 97.11°E	30	8.6 (HRV)	74.2
2007-09-12	10:26.8	4.44°S, 101.37°E	34	8.5 (GCMT)	75.2
2010-05-09	59:42.4	3.73°N, 96.08°E	61	7.2	74.0
2010-06-12	26:50.4	7.70°N, 91.98°E	35	7.5	72.4

The duration of faulting as given in Table 1 was estimated from the duration of the P-wave signal. If the P-wave radiation at the source continues for a time longer than the travel time difference between the P- and the S-wave for a given epicentral distance, the S-wave arrival with its typically large amplitudes may mask the continuing P-wave, and the duration of the faulting process may thus be biased. The duration in Table 1 thus signifies only a lower bound.

The value of the seismic moment magnitude ($M_w = 9.1$) is a matter of debate; published values range from 8.5 (IRIS) to 9.3, with $M_w = 9.2$ being considered as the most likely one. See Rhie et al[8]. An estimate of the accuracy of the seismic moment magnitude is not possible at this time, as no generally accepted procedure for the determination of this magnitude exists. The accuracy of other, conventional magnitudes published for earthquakes is also unknown. The range of scatter appears to be similar for both the conventional and the moment magnitudes.

2 Data

From the wealth of broadband seismograms of the Sumatra-Andaman earthquake examined here, 68 vertical-component seismograms with best signal-to-noise ratio have been selected for the present study. The epicentral distances of the respective stations are limited to the range from 60° to 95° thus assuring that the P-wave radiation is recorded as completely as possible, with a minimal distortion from the S-wave arrival. The distribution of the 68 stations surrounding the

epicenter is shown in Fig.1(a), together with the fault ruptured during the earthquake. As could be expected, the distribution of the stations is not even with respect to their azimuths, the highest density of stations being seen in the north-westerly sector (sector VI in Fig.1(a)), towards Europe. The largest gap in the azimuthal coverage occurs in sector IV. Fig.1(b) shows the positions of five reference earthquakes relative to the Sumatra-Andaman earthquake.

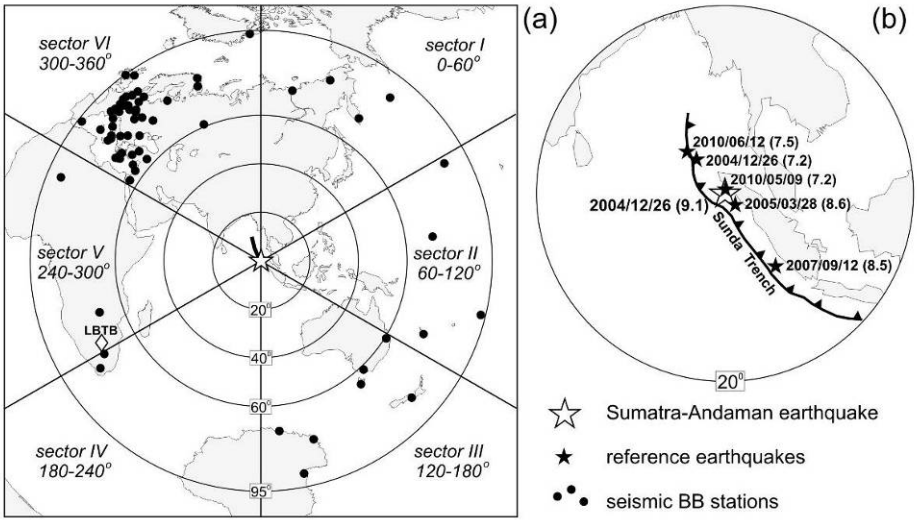

Fig.1 (a) Distribution of 68 seismic broadband stations (black dots) surrounding the epicenter of the Sumatra-Andaman earthquake (open star at the center). The thick line starting at the epicenter has a length of ca. 1 200 km and marks the fault ruptured during the earthquake (Banerjee et al[3]). The diamond indicates the station LBTB. (b) The location of the Sumatra-Andaman earthquake (open star) and of the epicenters of five reference earthquakes (black stars). The Sunda Trench subduction zone is taken from Bird[9]

In Fig.2, as examples of the broadband seismograms analyzed, the vertical-component record of the Sumatra-Andaman earthquake and of the five reference earthquakes are shown, as they were obtained at the station LTBT. The station is located in Botswana (Lobatse). It falls into sector V of Fig.1(a). The station LBTB is equipped with a borehole seismometer (Geotech Model KS-54000-IRIS), located 100 m below the Earth's surface. According to the manufacturer, the instrument is designed for ultra low-noise observations in the frequency band from 0.003 to 5 Hz (period range 0.2～300 s), i.e. the passband of the instrument has a width of nearly 11 octaves, and the absolute bandwidth amounts to nearly 5 Hz. In this band the instrument magnifies the ground velocity by a constant factor. The station proved to be operated at a site with an exceptionally low background noise.

The station LBTB is situated at an azimuth of about 90° with respect to the strike of the fault and at a distance of 73.7° from the epicenter of the Sumatra-Andaman earthquake (Fig.1(a)). Thus, the arrival times of the seismic phases are only minimally biased by the source moving along the fault during the rupture process, and the time differences of arrivals corresponding to radiation episodes at different points along the fault will predominantly reflect the time succession of the individual rupture episodes of the earthquake. The epicentral distances of the reference earthquakes from the station LBTB range from 72.4° to 75.2°, i.e. they deviate by not more than 1.5° from the epicentral distance of the main earthquake. For the epicentral distances of all earthquakes considered, the P- and S-waves are separated in time by about 10 minutes.

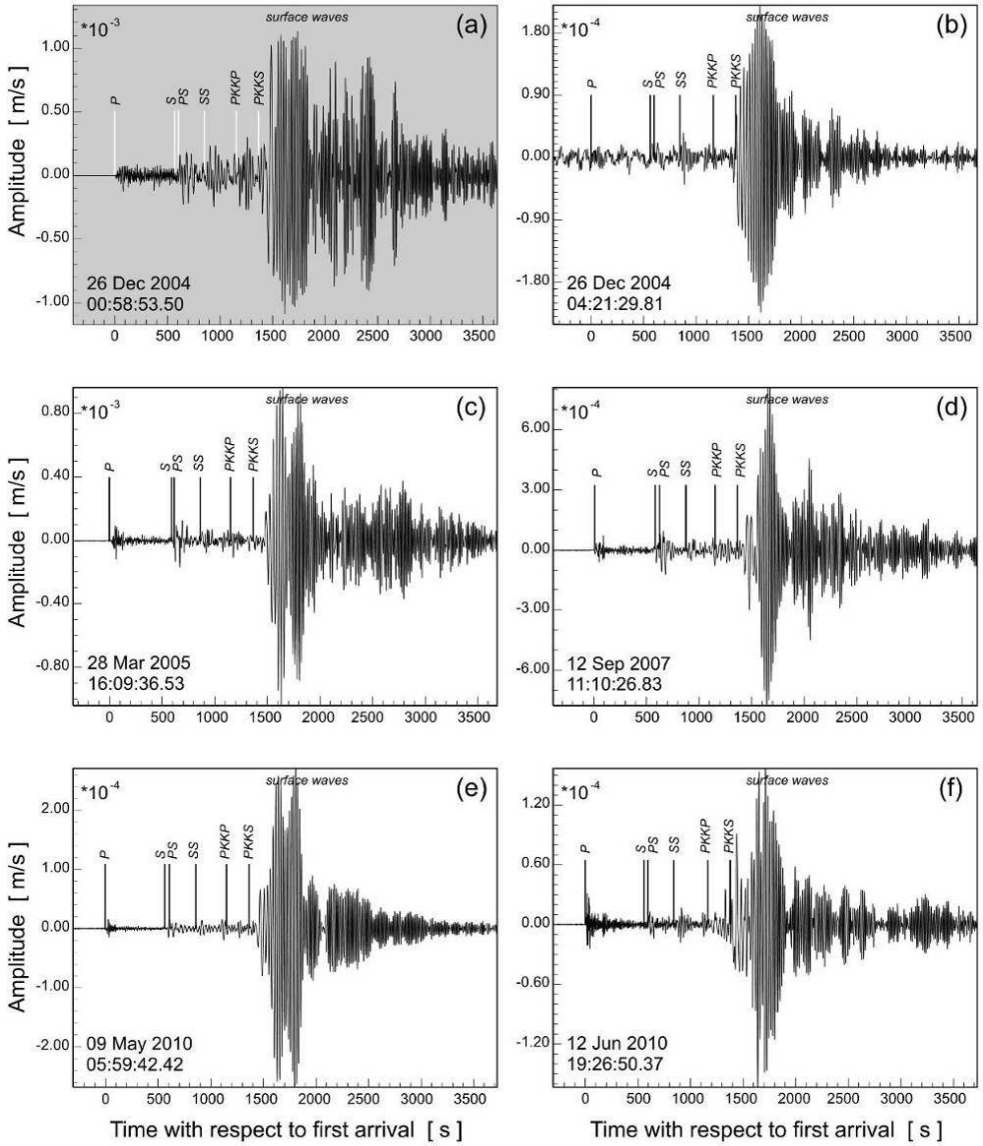

Fig.2 Vertical component broadband seismogram of the Sumatra-Andaman earthquake of 2010-12-26 (a), and of five reference earthquakes ((b)~(f)) recorded at the station LBTB. For details concerning the earthquakes see Tables 1 and 2

The seismograms of the Sumatra-Andaman earthquake in Fig.2(a), and of the reference earthquakes in Fig.2(b)~(f) have the length of one hour, starting just prior to the respective first P-wave arrivals. For the earthquake in Fig.2(a), the P-wave arrival is followed by a strong oscillation pattern continuing up to at least the S-wave arrival. For the largest aftershock of this earthquake the respective two arrivals are seen in Fig.2(b) to be disturbed by the coda of the previous shock. Disregarding the aftershock, the records of the earthquakes in Fig.2 show easily identifiable P-, S-, PS-, SS-, PKKP- and PKKS-phases. The phases are followed for all six earthquakes by a complex, large-amplitude surface wave train. The parameters of the earthquakes in Fig.2 are given in the Tables 1 and 2.

3 Analysis of broadband seismograms of body waves

For the sake of the following discussion distinction is made between several categories of events. Each event is associated thereby with a partial process in the focus of the given earthquake. The earliest event in the focus demonstrates itself as a rule in the form of the first P-wave arrival. This event may or may not be the strongest one of the earthquake. Also, it may or may not be the sole event associated with the earthquake.

In the case of the Sumatra-Andaman Earthquake the earliest event proves to be neither the strongest nor the sole one of the earthquake process.

The earliest event (primary event) is followed by subevents during the whole duration time of the earthquake. The subevents may have variable relative strengths, and variable spectral compositions. If the earliest event is not the strongest one, a subevent will qualify correspondingly. The latter is called the main event (arrow 4 in Fig.5; see also Table 3).

Table 3 Arrival times and frequencies of maxima indicated in the spectral seismograms of Fig.5(b) (station LBTB) and of Fig.6(b) (stacked of stations in the distance range 60°～95°)

From Fig.5(b)				From Fig.6(b)				
1	2	3	4	5	6	7	8	Arrival Interpretation
No.	Time /s	*f* /Hz	*T* /s	No.	Time /s	*f* /Hz	*T* /s	
1	7	0.144	6.94	1	23	0.220	4.55	first-arrival P-wave
2	28	0.150	6.67	2	39	0.200	5.00	P-wave of subevent
3	49	0.125	8.00	3	63	0.150	6.67	P-wave of subevent
4	73	0.050	20.0	4	94	0.054	18.5	P-wave arrival of main event, split into two subevents
4[x)]	95	0.072	13.9	—	—	—	—	second subevent of main event (see Fig.5c)
5	81	0.180	5.56	5	103	0.170	5.88	P-wave of subevent
6	135	0.120	8.33	6	154	0.073	13.7	P-wave of subevent
7	151	0.017	58.8	7	175	0.018	55.5	longperiodic P-wave arrival
—	—	—	—	8	243	0.082	12.2	P-wave of subevent (though the arrival time lies within the limits of the PP-wave, the frequency content is alien to that of the main P-wave, and the interpretation as PP-wave is rejected)
—	—	—	—	9	266	0.060	16.6	P-wave of subevent
—	—	—	—	10	282	0.140	7.14	P-wave of subevent
—	—	—	—	11	323	0.145	6.90	P-wave of subevent
—	—	—	—	12	350	0.054	18.5	P-wave of subevent (though the arrival time and the frequency content qualify the event as PPP-wave, the interpretation as PPP-wave is rejected, in view of no recognizable PP-wave)
—	—	—	—	13	355	0.046	21.7	P-wave of subevent
—	—	—	—	14	455	0.085	11.8	P-wave of subevent
—	—	—	—	15	621	0.100	10.0	P-wave of subevent
16	669	0.046	21.7	16	739	0.046	21.7	S-wave arrival corresponding to main event (arrow 4)
17	758	0.014	71.4	17	813	0.026	38.5	S-wave arrival corresponding to P-wave (arrow 7)
18	775	0.065	15.4	18	825	0.085	11.8	P-wave of subevent

1—Arrival in LBTB-seismogram; 2—Delay of maximum with respect to first-arrival P-wave; 3—Frequency of maximum; 4—Period of maximum; 5—Arrival on stacked seismogram; 6—Delay of maximum with respect to first-arrival P-wave; 7—Frequency of maximum; 8—Period of maximum

The main event, whether being the earliest event or a subevent, carries most of the seismic energy radiated in a single event of the earthquake. Seismographs with low magnification may record only the main event, which may lead to inconsistencies of the measured P-wave arrival times of the earthquake.

An earthquake, especially a strong one, is thus generally composed of a multitude of events occurring subsequently to the earliest event. From observations it appearts that the subevents occur at discrete times after the earliest event, but the focal process seems to come to a halt before the aftershocks sequence begins. Aftershocks are recognized as individual earthquakes occurring in the vicinity of the focal zone of the main shock. The aftershock sequence continues usually for a time substantially longer than the duration of the main shock, i.e. the time between the earliest event and the last subevent.

In the following, attention is focused on the first 900 s of the broadband seismogram of the earthquakes. This time window contains theoretically the P- and S-waves, as well as the earlier reflected, refracted and converted waves arriving at each station. Fig.3(a) shows an enlargement of the respective portion of the broadband seismogram of the Sumatra-Andaman earthquake of Fig.2(a). The first-arriving P-wave is seen to have a clear though low-amplitude onset in the compressional mode (upward movement). This P-wave corresponds to a relatively small energy burst, and its S-wave (with the arrival time marked by the respective vertical line) is not distinguishable as such from the seismogram. On the other side, the large-amplitude S-wave seen in the seismogram corresponds to the main P-wave arrival, which is delayed with respect to the first arrival by about 30 s. Both, this large-amplitude P-wave and its large-amplitude S-wave represent the strongest energy burst during the entire rupture process accompanying the earthquake, i.e. they represent the principal event of the earthquake. The phases secondary to the first-arrival P-wave in Fig.3(a), though also marked (pP, PcP, PP, PPP, S, PS), are not identifiable. This is due to the strong oscillations evidently produced by the faulting process continuing throughout most of the time window.

The broadband seismogram of Fig.3(a) is subjected to bandpass filtering. Butterworth filters of order 2 are applied, covering three frequency ranges: 1～5 Hz, 0.1～0.5 Hz, 0.01～0.05 Hz (corresponding period ranges: 0.2～1 s, 2～10 s, 20～100 s). The three filters have a common bandwidth of 2.5 octaves (absolute bandwidth: 4 Hz, 0.4 Hz, and 0.04 Hz, respectively). The bandpass seismograms in Fig.3(b), c, d correspond roughly to short-, medium- and long period recordings on conventional seismographs. All seismograms in Fig.3 are shown with the same velocity-amplitude magnification, i.e. the amplitudes of the waves can be compared directly with one another.

Needless to say that the bandpass seismograms of the Sumatra-Andaman earthquake in the figure are still difficult to interpret for individual arrivals in the range between the P- and S-wave arrivals. The difficulty to recognize individual arrivals (except for the first arrival) increases with frequency, the long period seismogram having the simplest appearance. The complexity of the short period (Fig.3(b)) seismogram relative to the complexity of the medium- and long period seismograms (Fig.3(c) and (d)) is due in part to its larger absolute bandwidth (4 Hz), compared to the bandwidths of the medium- (0.4 Hz) and the long period (0.04 Hz) seismograms. An analogous conclusion applies if the medium- and long period seismograms are compared with one another. In Fig.3(d), arrivals at times closely corresponding to the PP- and PPP-waves from the first-arrival P-wave are identified. The arrivals can not be interpreted as reflections of the P-wave however, because their frequency contents differ from that of the first-arriving P-wave. They can instead be understood as bursts of energy coincidentally arriving at the predicted arrival times of the PP- and PPP-waves.

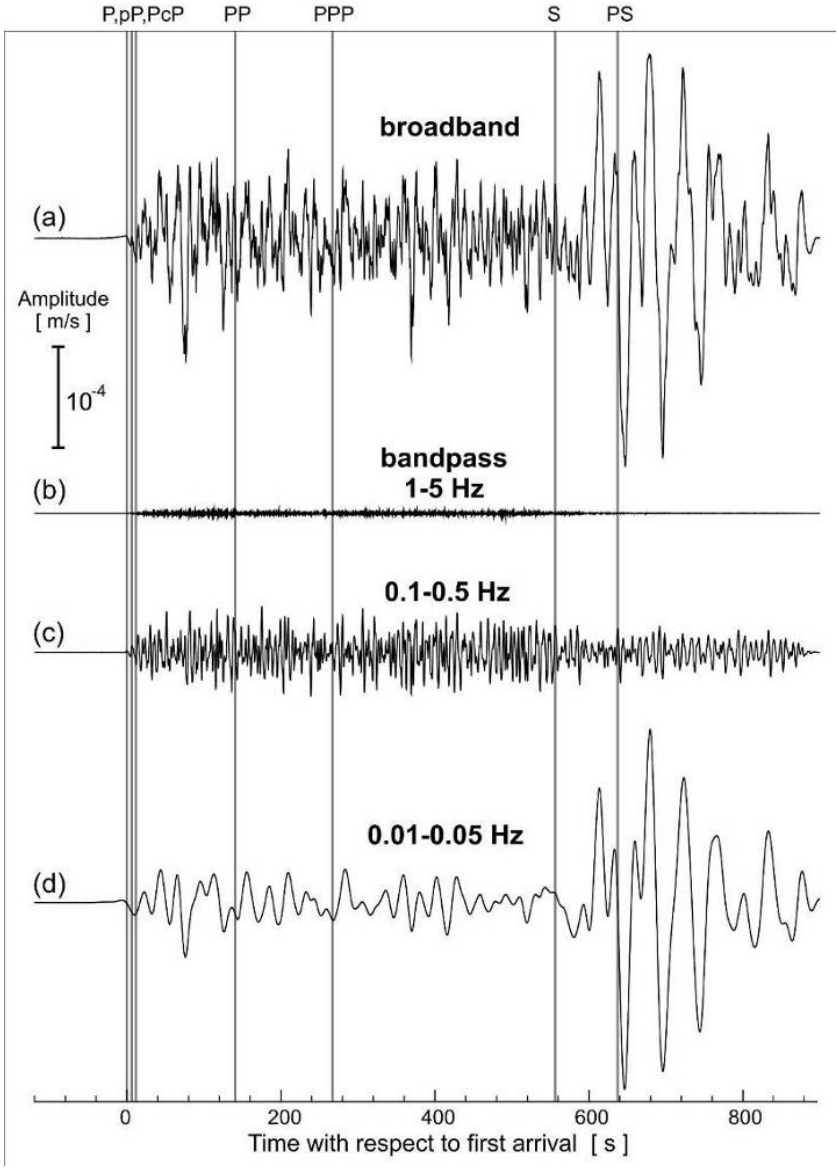

Fig.3 Vertical component broadband (a) and bandpass ((b)~(d)) seismograms of the first 900 s of the Sumatra-Andaman earthquake seismogram from Fig.2a. The theoretical arrival times of the P- and S-waves and the secondary phases in the given time window are indicated (Jeffreys and Bullen[10]). All traces have a common magnification

The records in Fig.3 indicate thus that in the time window considered the energy release occurred in two main stages, the large-amplitude burst — constituting the main part of the rupturing process — being delayed with respect to the first, smaller burst by about 30 s. The epicentral coordinates and the origin time, as given in Table 1, pertain only to the first, small-amplitude burst of energy. This earliest burst may have acted as the trigger for the main burst. In view of no exact definition of foreshocks, the early burst can eventually be addressed as the latest foreshock of the earthquake. The difference in the frequency contents of the two bursts is discussed in Section 6. The origin time and the location of the second event can not be

determined with the same accuracy as those of the first one, evidently as result of the lower accuracy with which the arrival time of the P-wave from the second, main event can be measured. Thus, the delay and the location of the second event with respect to the first one can be determined within only liberal error limits. A full quantification would require the individual origin times, locations, and other parameters of all individual subevents be given. However, no further details concerning the additional energy bursts can be recognized reliably from the broadband record in Fig.3(a), nor from the bandpass seismograms in Fig.3(b), (c) and (d).

The complexity of each seismogram in Fig.3 (b), (c) and (d) can be understood in terms of the number of Fourier-components accommodated in each bandpass, the number being largest for the widest, short period band (Fig.3(b)), and lowest for the narrowest, long period band (Fig.3(d)). This finding can be appreciated immediately from the amplitude density spectrum of the broadband seismogram of Fig.3(a). The spectrum of the ground velocity is shown in Fig.4, together with the frequency ranges corresponding to the bandpass seismograms of the Fig.3(b), (c) and (d), respectively. The dynamic range of the signals in the given frequency range extends thereby over 5 orders of magnitude (100 dB).

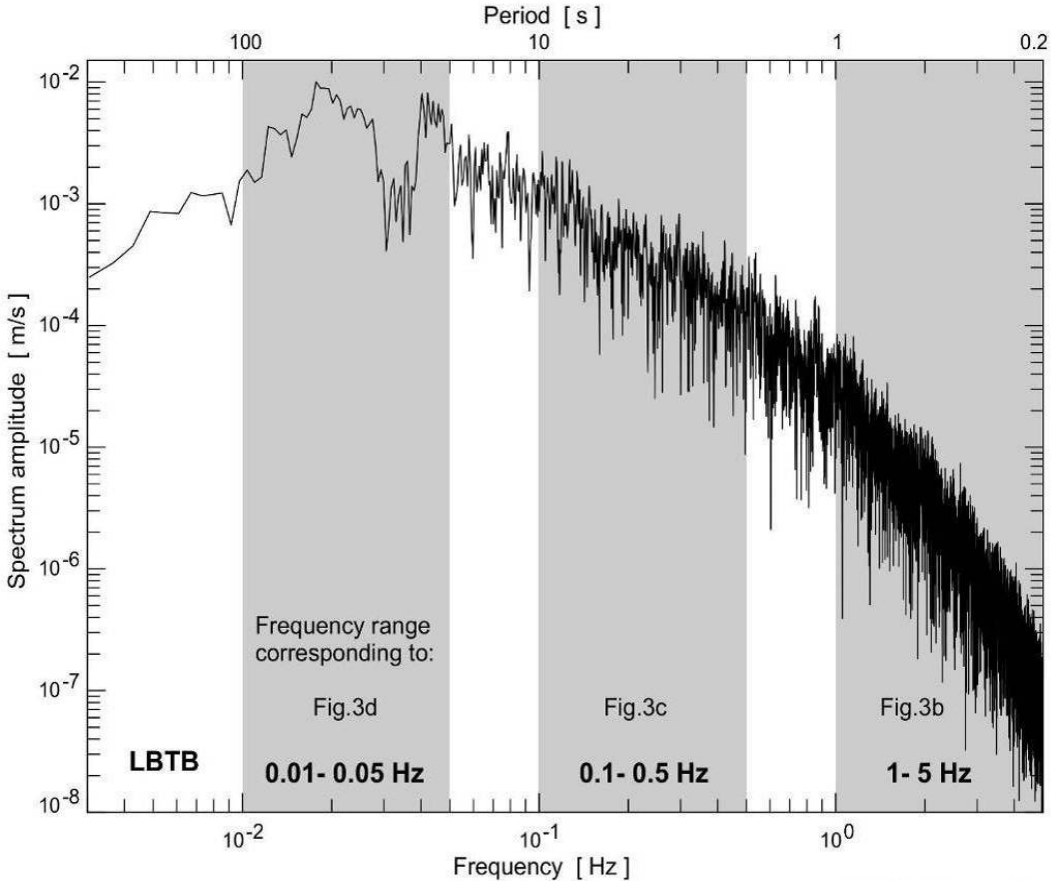

Fig.4 Velocity amplitude density spectrum for the broadband seismogram of Fig.3(a). The shaded areas indicate the frequency ranges corresponding to the bandpass seismograms in Fig, 3(b), (c) and (d)

The velocity amplitude density spectrum in Fig.4 shows only one half of the information which is contained in the broadband seismogram, as the phase spectrum is disregarded. The phase

spectrum, as a partial representation of the signal, is not amenable for a useful interpretation. Nonetheless, the amplitude density spectrum, especially the level of its horizontal tangent, has long been the basis for the quantification of the strength of an earthquake in terms of the scalar seismic moment of the event.

4 Spectral seismograms of the Sumatra-Andaman earthquake

Earlier, Duda et al[11] introduced spectral seismograms as a means to analyze broadband seismograms of seismic events. With the help of spectral seismograms a wealth of earthquakes and explosions has been interpreted (Duda and Xu[12]). On this background, spectral seismograms of the Sumatra-Andaman earthquake are given consideration for the purpose of elucidating details of the faulting process of the earthquake.

Based on the broadband record of Fig.3(a), three spectral seismograms are obtained (Fig.5(b), (c) and (d)). For the computation of each spectral seismogram, a set of 170 Butterworth filters of order 2 is applied to the record, the filters in each set differing from each other in their bandwidths (0.5, 0.3 and 0.1 octaves), as indicated in the figures. The order of the filter controls the steepness of the flanks of the filters, and the three bandwidths control the frequency resolution of the individual seismograms. Both, the filter order and the bandwidths, were chosen here in accordance with earlier practical experience (Duda and Xu[12], Duda and Kaiser[13], Fasthoff and Guo[14]). For a given bandwidth (0.5, 0.3 or 0.1 octaves), the outputs of each one of the 170 partially overlapping Butterworth filters yield a bandpass seismogram. Each of the seismograms is assigned to the midband frequency of the given filter. The arrangement of the 170 seismograms produces a representation of the broadband seismogram in the time and frequency domain. Subsequently, the absolute value of the outputs is taken, and the envelope of each set is computed. The respective envelopes are shown in the Fig.5(b), (c) and (d). From the comparison, and as theoretically expected, it is seen that the Butterworth filters with largest bandwidth (0.5 octave) yield a better time-resolution of the onset of each energy burst, at the expense of the frequency-resolution, whereas the smallest bandwidth (0.1 octave) enhances the frequency resolution of the record, in turn at the expense of the time-resolution (Jenkins and Watts[15]).

The total range of frequencies in each of the spectral seismograms in Fig.5 extends from 0.003 to 5 Hz (0.2～300 s). The range within which seismic energy arrives at the station is seen to be even smaller. However, due to the limited dynamic range of the chosen color presentation, amounting to about 40 dB, information is lost at high frequencies. As will be shown in Section 7, measurable seismic energy arrives for this earthquake at frequencies higher than 1 Hz.

As theoretically expected (Aki and Richards[16]), the maximum amplitude of a given phase depends on the bandwidth of the filter. Consequently, the maximum amplitudes in Fig.5b (obtained with filters 0.5 octave wide) are seen to be systematically larger (darker color of maxima) than in Fig. 5(c) (obtained with filters only 0.1 octave wide). It is noticed that amplitudes (e.g. of the P-phase) measured for the purpose of finding conventional magnitudes in seismological practice, are as a rule not compensated for the variable bandwidths of the seismographs utilized. Thus, the lack of consistence of the bandwidths contributes to the scatter of magnitude figures observed. The effect was found already by Båth[17], in course of the determination of mb-magnitudes. Records from a seismometer-galvanometer combination with a narrower total bandwidth yielded smaller magnitude figures, and vice versa. Also, the earthquake magnitude found from the duration of the wave train on a seismogram (duration magnitude), may be biased by the bandwidth of the seismograph. As a rule, narrowband seismographs yield longer durations, than these featuring a broader band, even if the midband periods are the same.

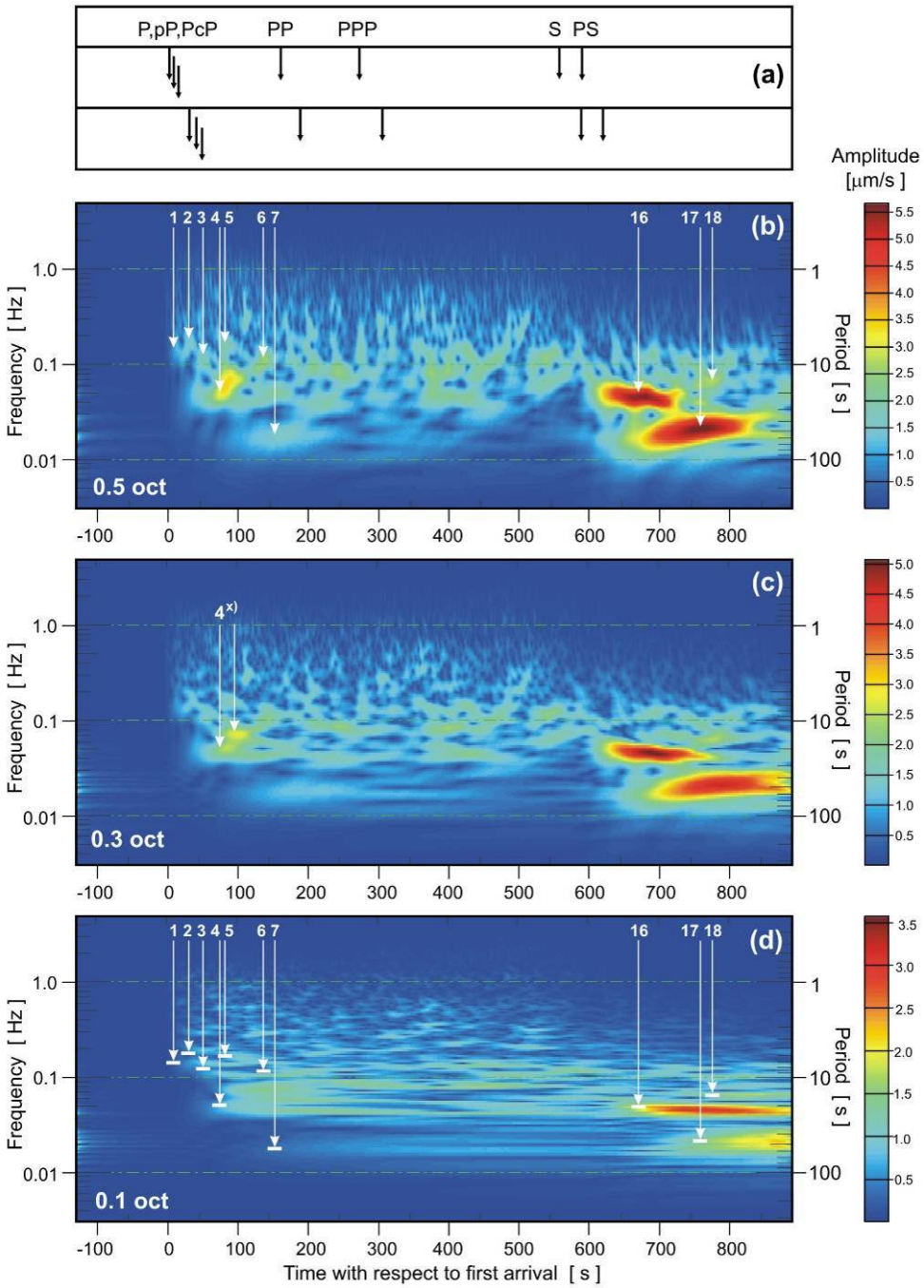

Fig.5 Spectral seismograms obtained from the broadband seismogram of the Sumatra-Andaman earthquake from Fig.3(a) (LBTB station). The spectral seismograms were obtained by applying Butterworth filters with the widths of 0.5 (b), 0.3 (c) and 0.1 (d) octaves, as indicated. Vertical arrows in the two uppermost rows (a) indicate the theoretical arrival times of the P, pP, PcP, PP, PPP, S and PS phases (upper row) and the same phases delayed by 30 s (Jeffreys and Bullen[10]). The vertical arrow 1 in (b) and (c) indicate the expected arrival of the P-wave, based on the origin time from Table 1. The vertical arrows 2 ~ 18 point to the maxima of the strongest energy bursts during the first ca 15 min of the record

In Fig.5(b), (c) and (d) the expanses of blue color signify “quiescence” i.e. no ground motion in the respective time and frequency ranges is observed with sufficient amplitudes. The expanses in other colors signify a “topography” produced by the ground motion induced by the energy arriving from the earthquake at the respective time and frequency. The cut-off amplitude thus lies about 40 dB (the range of the color scale) below the maximum amplitude occurring within the given time-frequency window, and the following conclusions apply only to arrivals within this dynamic range. During the few minutes preceding the first P-wave arrival, quiescence prevails in the total frequency range analyzed (0.003～2 Hz, i.e. 0.5～300 s). The quiescence is interrupted at the moment of the first arrival, with the “topography” rising quickly above the level of quiescence. The “topography” continues with time and in the frequency range from about 0.007 to about 1 Hz (1～150 s). Below and above this range quiescence prevails even after the first arrival. No discernible body wave energy is arriving at periods longer than about 150 s, and at periods shorter than about 1 s.

As the absorption of seismic waves is low at periods longer than 150 s, the quiescence is likely to signify here that no energy was radiated with sufficient intensity in this range in the form of body waves during the earthquake (Duda and Yanovskaya[18]). At periods shorter than about 1 s, the quiescence may be due to a lack of radiation with sufficient intensity, combined with a relatively strong absorption of the high frequency part of the respective body wave. High frequency radiation — if produced during the rupturing process — is suppressed during the propagation from the source to the station. It might have carried though originally a substantial part of the energy radiated, as well as significant information on the rupturing process. Below, a presentation is used, which visualizes the arrival of high frequency P-wave radiation at frequencies higher than 1 Hz.

The colors in Fig.5 are a measure of the ground velocity at the given time and frequency. Each one of the patches is an indication of the arrival of energy radiated in consequence of the faulting process during the earthquake. The possibility of P-wave energy arriving from sources unrelated to the earthquake is disregarded. The energy represented by the patches is arriving from a particular focus either directly along the shortest ray path, or as the result of multipathing. The energy patches in Fig.5(b), (c) and (d) are scaled with respect to the strongest velocity amplitude (arrow 17 in Fig.5(b), and arrow 16 in Fig.5(d)).

The arrivals indicated in Fig.5 by the arrows 16 and 17 are interpreted as two S-wave arrivals, the corresponding P-waves being assigned the arrows 4 and 7. The first-arrival P-wave (arrow 1), as found already above, has no identifiable S-wave, due to the relatively small amplitude of the corresponding energy burst. The absence of the S-wave is due to the high frequency radiation of this event, while the S-wave energy has been radically absorbed along the ray path. The strongest P-wave arrival (arrow 4) is seen in Fig.5(b) to start with a delay of about 30 s with respect to the first P-wave arrival. As previously mentioned, the first event may have triggered the massive event represented by the strongest P-wave. The latter can be recognized in Fig.5(c) to feature two maxima, separated in time by 22 s (Table 3).

If the second arrival is interpreted as a pP-wave of the first direct P, a depth of 55 km can be assigned to the focus of the main event. This interpretation is based on the travel time difference of the two events only, and disregards the difference in frequency (0.050 and 0.072 Hz respectively). See Table 3. Thus, this focal depth would require the assumption to be made that the source had pronounced directivity of radiation, the upward radiation (pP-wave) having had a clearly higher frequency than the downward radiation (P-wave). An alternative interpretation calls for the two maxima to represent two separate subevents within the main event of the earthquake, the later subevent featuring a higher frequency than the former. The

non-uniqueness of the interpretation is an example of the difficulty related to solving reverse problems in Seismology.

Fig.5 shows that the earthquake started with a small-amplitude, high frequency event (arrow 1). The main energy burst (arrows 4 for the P-wave, and arrow 16 for the S-wave) was delayed by 30 s, and radiated lower frequencies. Finally, after about 2.5 min, a long periodic radiation episode took place, with a clear P-wave (arrow 7) and S-wave (arrow 17). These three subevents were accompanied by smaller energy bursts, as indicated by the arrows 2, 3, 5, 6 in Fig.5(b). These patches are interpreted as evidence for secondary radiation episodes, generally occurring at higher frequencies than the main energy burst. In contrast to the P-wave (arrow 4), the S-wave of the main energy burst (arrow 16) shows only one maximum.

At times larger than the arrival time of the long periodic P-wave (arrow 7), a large number of energy bursts are seen over a wide range of frequencies. These bursts may represent direct arrivals from foci located along different sectors of the fault plane. They may also represent reflections and refractions of direct waves, or diffractions from heterogeneities inside the Earth. The interpretation of all details in these parts of the spectral seismogram in Fig.5 would be futile. Instead, in the following section the most persistent arrivals will be identified, based on a stack of the spectral seismograms of all broadband stations in Fig.1.

5 Stacking of spectral seismograms

Spectral seismograms for particular stations, as e.g. in Fig.5(b), (c) and (d), reveal a substantial complexity. It is likely that the complexity is due in part to the propagation along the specific ray path between the focus and the station. In order to minimize the effect of propagation, and in order to emphasize the effect of the focal process, stacking of spectral seismograms from a multitude of seismic stations is applied. At variance with ordinary seismogram stacking in the time domain, as employed e.g. in seismic prospecting, the stacking here is done in the time-frequency domain. It is expected that the spectral seismogram resulting from stacking will show the most robust energy bursts in the focus, de-emphasizing thereby incidental effects due to the propagation along the particular ray path.

Here, the propagation of seismic waves is assumed to be a purely linear process. This assumption implies that no frequency alteration of the wave leaving the focus takes place during its propagation. Thus multipathing and mode-conversion － if present － must lead to energy bursts with the same frequency content as that of the primary wave (disregarding the effects of selective absorption during the propagation along the paths). If the primary and the subsequent energy burst contain different frequencies, the subsequent burst can not be the result of multipathing or mode-conversion, and the burst must be interpreted in terms of a new subevent. If however the frequency contents of the primary and the subsequent burst do coincide, only the difference of arrival times may serve as a criterion for the true nature of the later arrival. Interpretation becomes difficult if the energy burst from such a subsequent event occurs at a time corresponding to the arrival time of a later phase of the primary event.

Spectral seismograms of the Sumatra-Andaman earthquake, as in Fig.5(b), (c) and (d) for the station LBTB, are stacked for 68 seismic stations with epicentral distances ranging from 60° to 95° from the epicenter (Fig.1). The seismograms are aligned according to the respective first-arriving P-wave. In Fig.6(a) (upper part) the arrows indicate the theoretical arrival times of the respective phases for the epicentral distance of 77.5°, while the horizontal bars mark the range of arrival times for 60°～95°. See Jeffreys and Bullen[10].

In Fig.6(a) (lower part) the respective times are shown relative to the main P-wave arrival

(arrow 4 in Fig.5). The result of stacking the spectral seismograms is shown in Fig.6(b), (c) and (d) for the filter widths indicated. Based on arrival times only, the energy bursts marked by arrows 8 and 12 could be interpreted as representations of the PP- and PPP-wave of the main P-wave (arrow 4). However the frequency content of the earlier burst (arrow 8) is alien to that of the main P-wave, and thus it likely represents an event of its own. Also, in view of the fact that the amplitude of arrival 12 (possible PPP-wave) is clearly stronger than that of the arrival 8 (possible PP-wave), the interpretation of both arrivals as reflected waves seems doubtful, and we favor the interpretation that these arrivals represent two unique subevents of the Sumatra-Andaman earthquake. None of the other arrivals prior to the S-waves qualifies as evidence of a reflected wave. Thus, the spectral seismograms in Fig.6 can be understood as representing a total of 15 events in the dynamic range of 40 dB below the strongest event (arrow 4) prior to the S-wave arrival. The latter is likely to consist of two subevents (16, 17), as seen in Fig.5(b), and as supported by the split of the frequencies of the event in Fig.6(b) and (d). Event 18, observed during the S-wave time window (16, 17) is characterized by higher frequency (0.08 Hz against 0.02 and 0.04 Hz for S-waves) and smaller energy (small amplitudes). Therefore it could be interpreted as a new P-wave subevent. Further subevents at even later times — if present — are masked by strong oscillations following the S-wave arrivals (arrows 16 and 17).

6 Duration of the Sumatra-Andaman earthquake

Generally, the duration of an earthquake may be understood as the time interval within which seismic energy is radiated from the source in the form of a given body wave. With this understanding the duration may be different for P- and for S-waves, and the relation between the two durations may become a matter of interest. It is shown below that the duration so understood depends on the dynamic range of the ground motion, as also on the frequency range taken into consideration.

Indeed, from Fig.5(b) it is seen that at frequencies below, say 0.1 Hz, the duration is restricted to that of the events marked by the arrows 4 and 7 for P-waves, and by the arrows 16 and 17 for S-waves, i.e. the durations in the form of P-waves and of S-waves respectively are fairly short. At higher frequencies the radiation is seen in the figure to be composed of numerous discrete energy arrivals. The duration of P-wave radiation here is longer. This can be also appreciated from the comparison of the Fig.3(d) with Fig.3(b): The duration of high-frequency P-waves clearly exceeds that of low-frequency P-waves.

Before looking at the radiation at still higher frequencies, we point to the dependence of the duration on the dynamic range: If in Fig.5(b) only a dynamic range of, say, one order of magnitude below the maximum were taken into account, the duration would be estimated to coincide with the duration of the main energy burst (arrow 4). Extending the dynamic range successively leads to longer durations. Consequently, disregarding the effects of frequency and of dynamic range yields duration estimates which may be biased.

Turning to the highest frequencies recorded on broadband seismographs, the spectral seismogram for the frequency range from 1 Hz to 5 Hz is shown in Fig.7(a). It was obtained from the broadband seismogram of Fig.2(a), applying a procedure analogous to that for obtaining the spectral seismograms in Fig.5 discussed earlier. In contrast to Fig.5(a) dominated by a synoptic sequence of arrivals at lower frequencies, Fig.7a shows a quasi-continuous radiation, composed of hundreds of individual subevents with frequencies in the range from 1 Hz to 5 Hz. The corresponding S-waves are not visible due to their strong

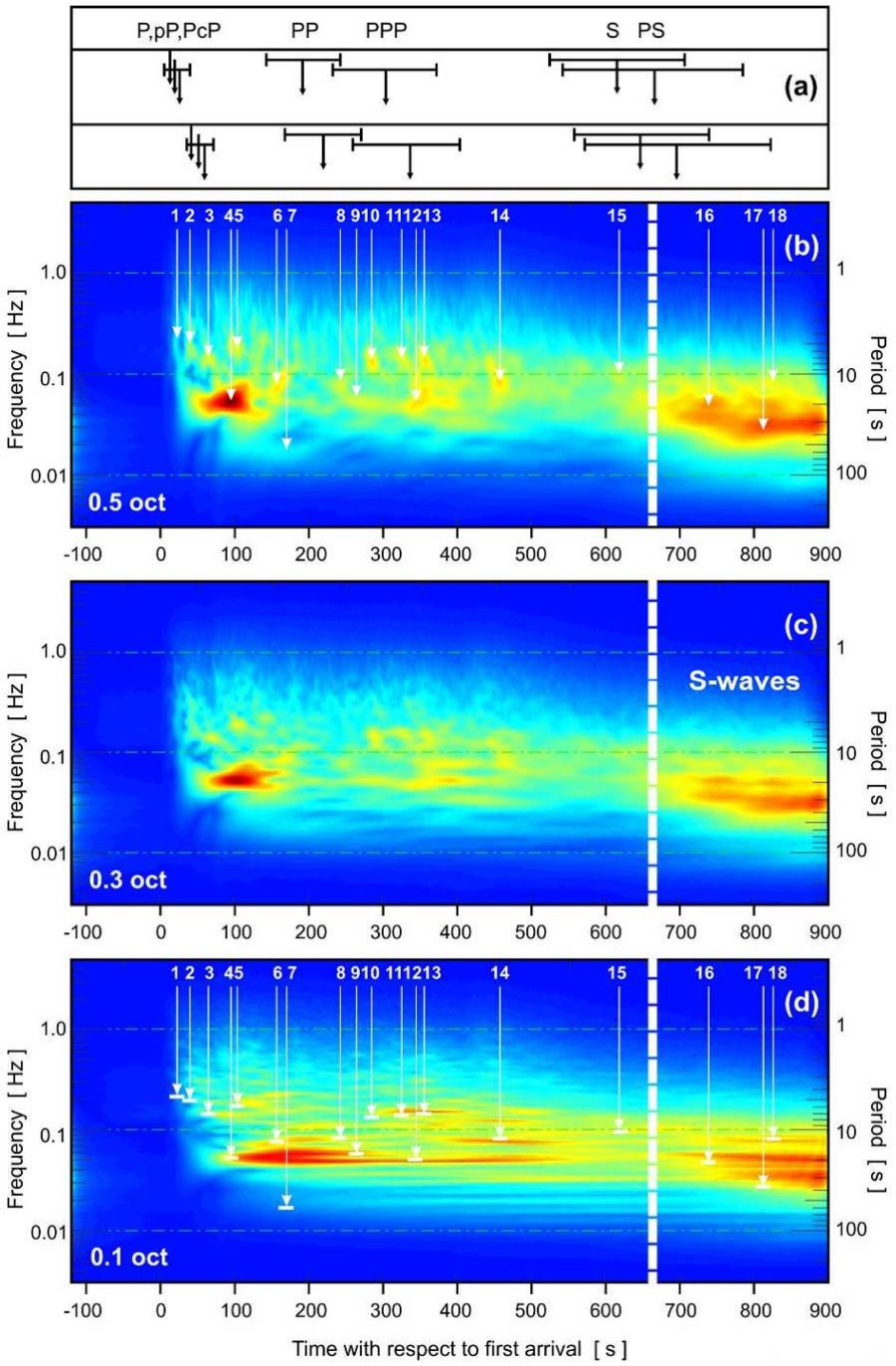

Fig.6 Spectral seismograms obtained by stacking the individual spectral seismograms from stations with epicentral distances in the range 60°～95° (Fig.1). Thereby the seismograms are aligned with respect to their expected arrival time of the P-wave at the stations calculated for iasp91 model (Kennett and Engdahl[19]). Vertical arrows in the two uppermost rows (a) indicate the arrival times of the phases for an epicentral distance of 77.5° (center of the distance range); indicated are also the ranges of the arrival times for the distance range 60°～95°. The spectral seismograms were obtained by applying Butterworth filters with the widths of 0.5 (b), 0.3 (c) and 0.1 (d) octaves, as indicated. The vertical arrows 1～18 point to the maxima of the strongest energy bursts during the first about 15 min of the record (see also Table 3)

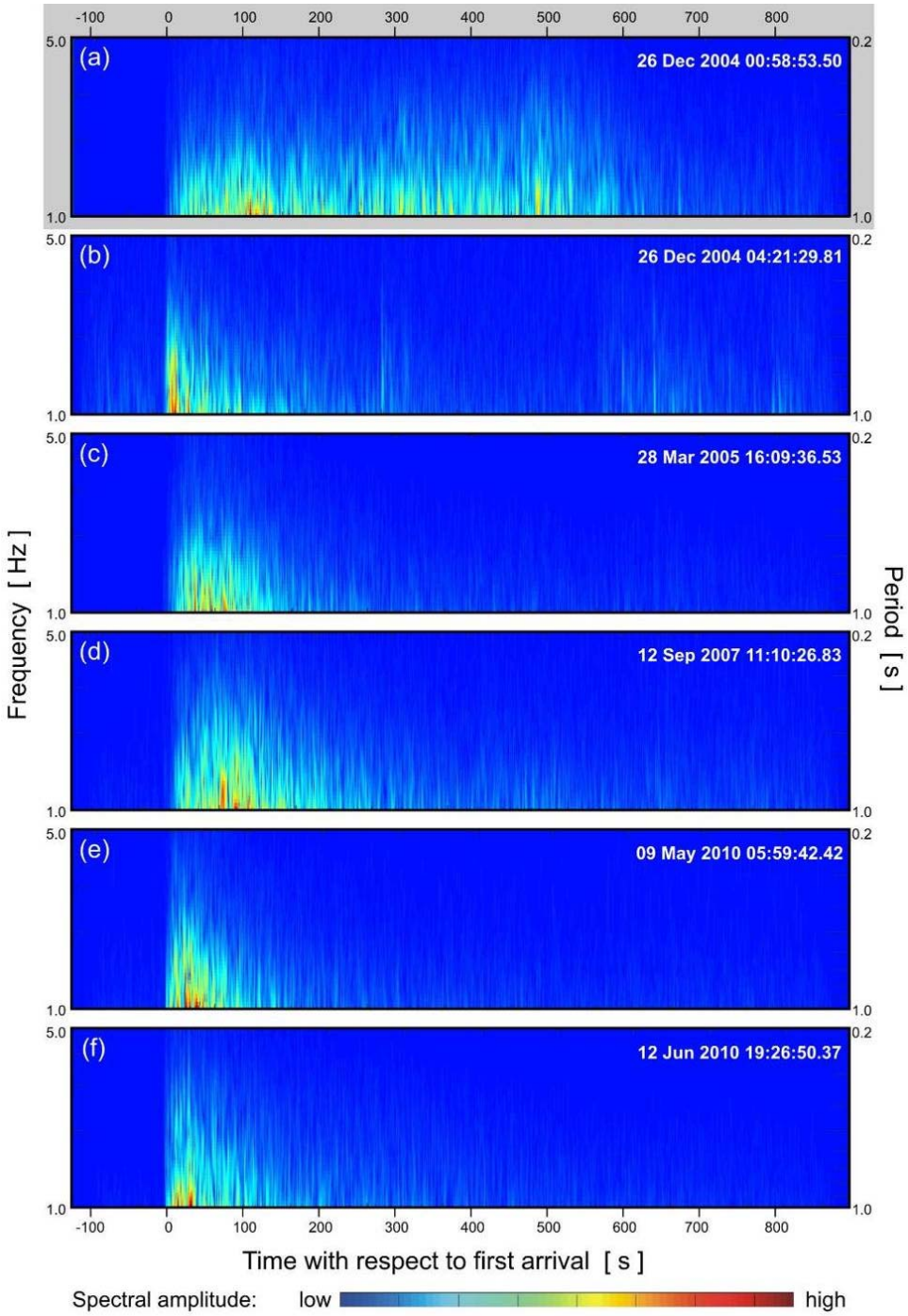

Fig.7 Spectral seismograms in the frequency range 1 ~ 5 Hz for the Sumatra-Andaman earthquake (a) and of five reference earthquakes (b) ~ (f)

absorption alongthe ray path. The P-wave radiation continues for estimated 10 minutes after the first-arrival P-wave (arrow 1 in Fig.5(b)), and apparently was triggered by the earliest event. It may be said that the sequence of subevents is equivalent to a “humming” at subsonic

frequencies. The intensity of radiation at these frequencies in the source must have been unusually strong, as the “humming” is recorded at a distance as large as 73.7°. Whether the “humming” continued for a time longer than 10 minutes, but at a lower intensity level, could be eventually found from broadband records obtained at local epicentral distances. This question, together with that concerning eventual “humming” in the S-wave mode, is however beyond the scope of the present investigation.

Similar features of spectral seismograms in the frequency range from 1 Hz to 5 Hz are seen for five reference earthquakes in the region (Fig.7(b)~(f)) computed from the bandpass seismograms of Fig.2(b)~(f). The duration of the P-wave trains for the reference earthquakes ranges from about 100 s up to about 270 s. See Fig.7.

Basically, the studies cited agree with our findings. They do not however recognize the substantially larger number of subevents, neither do they recognize the differences in their spectral contents, as it was possible in the present study employing spectral seismograms. In particular, the authors cited do not recognize the infrasonic “humming”, observed at extremely large epicentral distances, and－due to its high frequency content－estimated to correspond to a substantial part of the energy radiated during the earthquake.

Acknowledgement: The investigation was performed within the partnership agreement between the University of Warsaw and of Hamburg University. The GSAC-Generic Seismic Application Coding software (Herrmann and Ammon[23]) and the public domain GMT software (Wessel and Smith[24, 25]) have been used to preprocess the data and to produce some of the figures. The facilities of the IRIS Data Management System, and specifically the IRIS Data Management Center, were used for access to waveform and metadata required in this study. The IRIS DMS is funded through the National Science Foundation and specifically the GEO Directorate through the Instrumentation and Facilities Program of the National Science Foundation under Cooperative Agreement EAR-0004370. Professor Guo Lucan, Institute of Geophysics, CEA, Beijing, has shown keen interest in the investigation and has contributed to it by way of discussions on various occasions. All support is gratefully acknowledged.

References

[1] Duda SJ. 由地震和爆炸激发的地震 P 波层析成像——第一部分：基本概念与理论[J]. CT 理论与应用研究, 2007, 16(1): 25-34. (英文)
Duda SJ. Tomography of seismic P-waves from earthquakes and explosions－Part I: Basic Concepts and Theory[J]. CT Theory and Applications, 2007, 16(1): 25-34.

[2] Ammon CJ, Ji C, Thio KH, et al. Rupture process of the 2004 Sumatra-Andaman Earthquake[J]. Science, 2005, 308(5725): 1133-1139.

[3] Banerjee P, Pollitz FF, Burgmann R. The size and duration of the Sumatra-Andaman earthquake from far-field static offsets[J]. Science (New York, N.Y.), 2005, 308(5729): 1769-1772.

[4] Jeffrey P, Alex ST, Jeroen T, et al. Earth’s free oscillations excited by the 26 December 2004 Sumatra-Andaman earthquake[J]. Science, 2005, 308(5725): 11-39-1144.

[5] Thorne L, Kanamori H, Ammon JC, et al. The great Sumatra-Andaman earthquake of 26 December 2004[J]. Science, 2005, 308(5725): 1127-1133.

[6] Gusev AA, Guseva EM, Panza GF. Size and duration of the high-frequency radiator in the source of the 2004 December 26 Sumatra earthquake[J]. Geophysical Journal

International, 2007, 170: 1119-1128.
[7] Liu N, Chen QF, Niu FL, et al. Rupture of the 2004 Sumatra-Andaman earthquake inferred from direct P-wave imaging[J]. Chinese Science Bulletin, 2007, 52(14): 1986-1991.
[8] Rhie J, Dreger D, Bürgmann R, et al. Slip of the 2004 Sumatra-Andaman earthquake from joint inversion of long-period global seismic waveforms and GPS static offsets[J]. Bulletin of the Seismological Society of America, 2007, 97(1 A SUPPL.): S115-S127.
[9] Bird P. An updated model of plate boundaries[J]. Geochemistry, Geophysics, Geosystems, 2003, 4(3): 1027.
[10] Jeffreys H, Bullen KE. Seismological tables[M]. London, UK: British Association for the Advancement of Science, 1940: 50.
[11] Duda SJ, Nortmann R. Determination of spectral properties of the earthquakes from their magnitudes[J]. Tectonophysics, 1983, 93(3-4): 251-275.
[12] Duda SJ, Xu SX. Broadband seismograms, band-pass seismograms, and spectral magnitudes for a selection of 1978-1983 explosions-comparison with worldwide earthquakes[R]. Institute of Geophysics, University Hamburg.
[13] Duda SJ, Kaiser D. Spectral magnitudes, magnitude spectra, and earthquake quantification: The stability issue of the corner period and of the maximum magnitude for a given earthquake[J]. Tectonophysics, 1989, 166(1): 205-211.
[14] Fasthoff S, 郭履灿. 论震波频谱图—地震波的三维显示[J]. CT 理论与应用研究, 2001, 10(3): 47-51. (英文)
Fasthoff S, Guo LC. On spectral seismograms-3D display of seismogram[J]. CT Theory and Applications, 2001, 10(3): 47-51.
[15] Jenkins G, Watts DG. Spectral analysis and its applications[M]. San Francisco, USA: Holden-Day, 1968: 525.
[16] Aki K, Richards PG. Quantitative seismology: Theory and methods[M]. Vol. I and II. San Francisco, USA: W.H. Freeman and Company, 1980: 932.
[17] Båth M. Introduction to seismology[M]. Birkhäuser Verlag, Basel. Switzerland. 1973: 395.
[18] Duda SJ, Yanovskaya TB. Spectral amplitude-distance curves for P-waves: effects of velocity and Q-distribution[J]. Tectonophysics, 1993, 217(3-4): 255-265.
[19] Kennett B, Engdahl E. Traveltimes for global earthquake location and phase identification[J]. Geophysical Journal International, 1991, 105: 429-465.
[20] Krüger F, Ohrnberger M. Tracking the rupture of the M_w=9.3 Sumatra earthquake over 1,150 km at teleseismic distance [J]. Nature, 2005, 435(7044): 937-939.
[21] Tsai CV, Meredith N, Ekström G, et al. Multiple CMT source analysis of the 2004 Sumatra earthquake[J]. Geophysical Research Letters, 2005, 32(17): 1-4.
[22] Ishii M, Shearer MP, Heidi H, et al. Extent, duration and speed of the 2004 Sumatra-Andaman earthquake imaged by the Hi-Net array[J]. Nature, 2005, 435(7044): 933-936.
[23] Herrmann RB, Ammon CJ. GSAC Generic seismic application coding, (version 3.30): Computer programs in seismology[R]. 2007: 201.
[24] Wessel P, Smith WF. The generic mapping tools GMT (version 3): Technical reference and cookbook[M]. 1995: 77.
[25] Wessel P, Smith WF. The generic mapping tools GMT[J]. Reference manual pages. 1995(version 3).

地震和爆炸的 P 波层析成像
———第二部分：由时频地震图得到的 2004 年苏门答腊-安达曼地震的断层破裂特征

Monika WILDE-PIÓRKO[1], Seweryn J. DUDA[2✉], Marek GRAD[1]

1. Institute of Geophysics, Faculty of Physics, University of Warsaw, Pasteura 7, 02-093 Warsaw, Poland
2. Institute of Geophysics, Hamburg University, Bundesstrasse 55, 20146 Hamburg, Germany

摘要：本文分析了 2004 年 12 月 26 日苏门答腊-安达曼地震的宽频带地震图。目的是通过不同频率成分的子事件的发生时间了解断层的破裂过程。具体分析的是由相应宽频带地震记录得到的 P 波的时频地震图。分析结果说明，在 S 波到达前的时窗内发生了最大辐射强度的相应频率低于 1 Hz 的 15 次较大子事件，但在同样的时窗内，还发生了最大辐射强度的频率更高的数百次小事件，形成了准连续的次声频率的蜂鸣声，在远至 8 000 km 的距离上都还能观测到。由于高频波在射线传播路径上存在较强的吸收，因而可以断定，地震期间有一大部分的地震能量是以蜂鸣声的形式被释放了。

关键词：苏门答腊-安达曼地震；宽频带地震图；频谱地震图；地震能量的高频辐射；破裂持续时间

Biography: Monika WILDE-PIÓRKO (1972－), Female, Assistant Professor, Head of Lithosheric Physics Division, University of Warsaw, Warsaw, Poland. Research interest: Structural seismology, investigation of the crust and mantle using explosion and natural sources, Tel: +48 225546851, E-mail: mwilde@igf.fuw.edu.pl.

Seweryn J. DUDA✉(1933－), Male, Professor Emeritus, Hamburg University, Hamburg, Germany. Research interest: Earthquake Seismology, in particular Quantification of Earthquakes, Tel: +49 50662780, E-mail: seweryn.duda@zmaw.de.

Marek GRAD (1951－), Male, Professor, University of Warsaw, Warsaw, Poland. Research interest: Structural seismology, investigation of the crust and upper mantle using explosion and natural sources, Tel: +48 225546826, E-mail: mgrad@mimuw.edu.pl.